Chinese Chemical Letters 31 (2020) 1119–1123

Contents lists available at ScienceDirect

Chinese Chemical Letters

journal homepage: www.elsevier.com/locate/cclet

Communication

Controllable synthesis of highly crystallized mesoporous TiO_2/WO_3 heterojunctions for acetone gas sensing

Changyao Wang[a,1], Yuhui Li[a,1], Pengpeng Qiu[a], Linlin Duan[a], Wei Bi[c,*], Yan Chen[a], Dingyi Guo[a], Yupu Liu[a], Wei Luo[b,*], Yonghui Deng[a]

[a] Laboratory of Advanced Materials, Department of Chemistry, Shanghai Key Lab of Molecular Catalysis and Innovative Materials, iChEM and State Key Laboratory of Molecular Engineering of Polymers, Fudan University, Shanghai 200433, China
[b] State Key Laboratory for Modification of Chemical Fibers and Polymer Materials, College of Materials Science and Engineering, Institute of Functional Materials, Donghua University, Shanghai 201620, China
[c] Department of Stomatology, Zhongshan Hospital, Fudan University, Shanghai 200032, China

ARTICLE INFO

Article history:
Received 10 July 2019
Received in revised form 9 August 2019
Accepted 26 August 2019
Available online 26 August 2019

Keywords:
Mesoporous materials
Acetone gas sensing
Heterojunctions
TiO_2
WO_3

ABSTRACT

Mesoporous semiconducting metal oxides (SMOs) heterojunctions are appealing sensors for gas detecting. However, due to the different hydrolysis and condensation mechanism of every metal precursor and the contradiction between high crystallinity and high surface area, the synthesis of mesoporous SMOs heterojunctions with highly ordered mesostructures, highly crystallized frameworks, and high surface area remains a huge challenge. In this work, we develop a novel "acid-base pair" adjusted solvent evaporation induced self-assembly (EISA) strategy to prepare highly crystallized ordered mesoporous TiO_2/WO_3 (OM-TiO_2/WO_3) heterojunctions. The WCl_6 and titanium isopropoxide (TIPO) are used as the precursors, respectively, which function as the "acid-base pair", enabling the co-assembly with the structure directing agent (PEO-*b*-PS) into highly ordered mesostructures. In addition, PEO-*b*-PS can be converted to rigid carbon which can protect the mesostructures from collapse during the crystallization process. The resultant OM-TiO_2/WO_3 heterojunctions possess primitive cubic mesostructures, large pore size (~21.1 nm), highly crystalline frameworks and surface area (~98 m^2/g). As a sensor for acetone, the obtained OM-TiO_2/WO_3 show excellent response/recovery performance (3 s/5 s), good linear dependence, repeatability, selectivity, and long-term stability (35 days).

Mesoporous semiconducting metal oxides (SMOs) have been widely used as the resistive-based gas sensors due to its excellent properties such as high surface area, long-term stability, large pore volume, high interconnected and adjustable mesopores [1–6]. The high surface area can continuous offer countless bonding sites between target gas molecules and the surface-chemisorbed oxygen species (O^{2-}, O^- and O_2^-) on the sensing layer of mesoporous SMOs, improving the sensitivity of gas sensor [7–9]. In addition, the large pore volume, interconnected and adjustable mesopores are beneficial to the gas diffusion velocity in the mesoporous SMOs frameworks, improving the response/recovery rate and detection limit [10,11]. Up to now, a variety of strategies have been reported for the synthesis of mesoporous SMOs, such as sol-gel process [12–14], precipitation reactions [15–17], spray pyrolysis [18–20], and chemical vapor deposition (CVD) [21,22]. However, the low crystallinity and porosity of the obtained mesoporous SMOs by these methods can also lead to the poor electron conductivity and gas diffusion rate which is unfavorable for high performance gas sensor.

Constructing mesoporous SMOs with high crystalline framework, high surface area, and high electron conductivity is beneficial to the improved sensing performance [23]. However, the high crystallinity will also lead to the decreased surface area because the crystallization at high temperature will cause the damage of mesostructures [24–27]. By using hard-templating method, ordered mesoporous SMOs with high crystalline framework can be synthesized. However, this method is complicated and costly [28–34]. By contrast, the soft-templating method based on the cooperative assembly (co-assembly) between polymer and precursors is a simple and convenient route [35–37]. However, the low glass transition temperature of commercial polymers usually leads to mesoporous SMOs with low crystallinity framework which is unfavorable to the sensing performance [38–40]. In addition,

* Corresponding authors.
E-mail addresses: bi.wei@zs-hospital.sh.cn (W. Bi), wluo@dhu.edu.cn (W. Luo).
[1] These authors contributed equally to this work.

https://doi.org/10.1016/j.cclet.2019.08.042
1001-8417/

constructing SMOs heterojunctions was also regarded as the useful way to improve the electron conductivity of whole framework [41]. However, designing and fabricating mesoporous SMOs heterojunctions remains rare, which is mainly attributed to the defect of commercial polymers and the lack understanding of the various hydrolysis and condensation process of different metal precursors. Thus, reliable approaches for constructing mesoporous SMOs heterojunctions with high framework crystallinity and high surface area remain desirable.

Herein, we report the construction of highly crystalline OM-TiO_2/WO_3 heterojunctions through the "acid-base pair" adjusted EISA process. WCl_6 and titanium isopropoxide (TIPO) are used as the precursors, respectively, which function as the "acid-base pair" [42], enabling the assembly with PEO-*b*-PS into ordered mesotructrues. Notably, the "acid-base pair" was employed to adjust the hydrolysis and condensation process of used inorganic precursors, thus makes the co-assembly process more controllable. In addition, PEO-*b*-PS can be converted to rigid carbon which can protect the mesostructures from collapse during the crystallization process [1]. The resultant OM-TiO_2/WO_3 heterojunctions exhibits highly crystalline TiO_2/WO_3 heterojunctions frameworks, large pore size (~21.1 nm), high surface areas (98 m^2/g), and high pore volume (0.28 cm^3/g). When being used as a sensor for acetone, the OM-TiO_2/WO_3 heterojunctions show excellent response/recovery performance (3 s/5 s), outstanding linear dependence, repeatability, selectivity, and long-term stability (35 days).

The synthesis procedure of the crystalline OM-TiO_2/WO_3 heterojunctions is illustrated (Fig. S1 in Supporting information). First, 0.10 g of PEO_{117}-*b*-PS_{198} was added in 5 g of tetrahydrofuran (THF) with stirring to form a homogeneous solution. Meanwhile, 0.125 g of WCl_6 and 0.25 g of TIPO (molar ratio of WCl_6 to TIPO is 1:3) were added in 2 g of ethanol subsequently, forming the dark green solution after stirring for 0.5 h. Then, the dark green solution was mixed with the PEO_{117}-*b*-PS_{19} solution. After stirring for another 2 h at 25 °C, the obtained mixed solution was poured into petri dishes. After heat treatment at 100 °C for 24 h, the as made PEO-*b*-PS/W/Ti composites (denoted as as-made sample) can be obtained. Then the as-made sample was calcined at 350 °C for 3 h (1 °C/min) and 500 °C for 1 h (5 °C/min) in N_2, resulting in the carbon supported TiO_2/WO_3 heterojunctions (black powder) (denoted as OMC-TiO_2/WO_3). With further pyrolysis at 500 °C in air for 2 h (1 °C/min), the yellow green crystalline OM-TiO_2/WO_3 heterojunctions could be obtained. The other mesoporous TiO_2/WO_3 composites with different Ti/W ratio were synthesized through the same procedure of OM-TiO_2/WO_3 by adjusting the ratio of titanium and tungsten precursors. Mesoporous TiO_2 was prepared according to our previous report [27].

The fabricated gas sensor is shown in Fig. S2 (Supporting information). First, the obtained OM-TiO_2/WO_3 heterojunctions was mixed with terpineol to form a paste. Then the paste was coated on the alumina tube printed with a pair of Au electrodes. After heat treatment at 100 °C for 2 h and 500 °C for 2 h consecutively, the temperature control coil (Ni-Cr alloy) was added into the tube. Finally, the obtained sensor was further calcined at the working temperature for 7 days to improve the stability. The gas sensing measurements were implemented on the HW-30A test system (Fig. S3 in Supporting information). The gas sensing data was analyzed by the stationary-state gas distribution method. The voltage value of the load resistor changes with the amount of target gas and was recorded once time every second. The gas response was defined as the ratio of R_a and R_g (R_a/R_g). R_a and R_g are the resistance value of the sensor in air and testing gas (air and acetone), respectively. The response and recovery time were defined as the time of the output value reach to 90% of its saturation value after injecting and releasing the target gas, respectively.

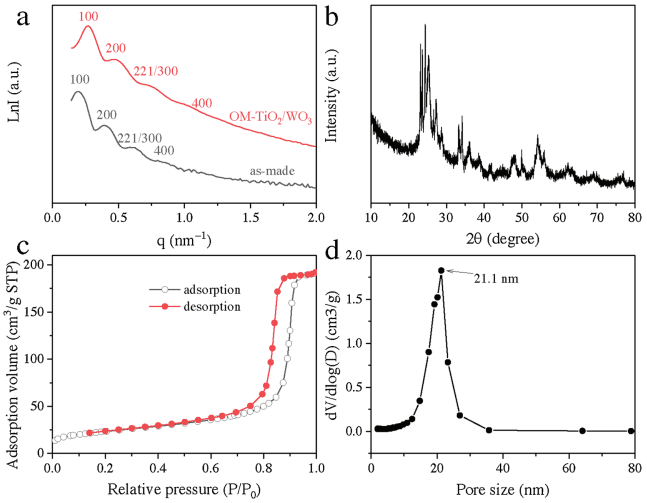

Fig. 1. (a) SAXS patterns of the as-made sample and OM-TiO_2/WO_3, respectively. (b) The XRD pattern, (c) Nitrogen-sorption isotherms and (d) pore-size distribution curve of the crystalline OM-TiO_2/WO_3 heterojunctions material obtained after heat treatment at 500 °C in air.

Four scattering peaks at q values of 0.194, 0.394, 0.591 and 0.779 nm^{-1} can be observed from the SAXS pattern of the as-made sample obtained after the evaporation at 100 °C (Fig. 1a). These peaks can be indexed as the [100], [200], [221]/[300] and [400] reflections of primitive cubic mesostructures, respectively. The unit cell parameter (a) of the as-made sample is calculated to be 32.4 nm by using the formula $d = 2\pi/q$ and $a = d_{100}$, demonstrating a large unit of the obtained mesostructures. After pyrolysis at 500 °C in air, the SAXS pattern (Fig. 1a) of the obtained material (OM-TiO_2/WO_3) still show four scattering peaks, demonstrating the highly stability of the ordered mesostructures. The value of first scattering peak is 0.268 nm^{-1}, attributing to the smaller unit cell parameter (23.4 nm). The mesostructures shrinkage percentage is calculated to be ~27.8%. In addition, the XRD pattern (Fig. 1b) of the OM-TiO_2/WO_3 heterojunctions displays several diffraction peaks that correspond to mixed anatase (JCPDS No. 21-1272), tungsten oxide (JCPDS No. 43-1035), and rutile (JCPDS No. 21-1276) phases, respectively, demonstrating the existence of TiO_2/WO_3 heterojunctions. The narrow and high intensities of the diffraction peaks demonstrate the high crystallinity of WO_3 and TiO_2 nanocrystals.

The FESEM image (Fig. 2a) clearly indicate that the obtained OM-TiO_2/WO_3 heterojunctions possess a large-domain ordered spherical pore array, which can be further observed from the transmission electron microscopy (TEM) images (Fig. 2b). Spotty diffraction pattern rings (Fig. 2c) belong to TiO_2 and WO_3 can be seen from the selected-area electron diffraction (SAED) pattern, demonstrating that the framework of the mesotructure is consisted of TiO_2 and WO_3 nanocrystals. Lattice fringes belong to the (101) plane of anatase TiO_2 (3.51 Å) and the (001) plane of orthorhombic WO_3 phase (3.85 Å) can be detected from the high-resolution transmission electron microscopy (HRTEM, Fig. 2d). Meanwhile, the TiO_2 nanocrystals connect with WO_3 nanocrystals tightly, demonstrating the existence of TiO_2/WO_3 heterojunctions. EDX spectra (Fig. S4 in Supporting information) show the coexistence of Ti, W, O elements in the OM-TiO_2/WO_3. The content of each element is listed in the Table S1 according to the EDX analysis. The atomic ratio of Ti to W is 2.8:1, which is basically in agreement with the mole ratio of titanium and tungsten precursor of 3:1. According to the Table S1 (Supporting information), the O, Ti and W atom percentage are 47.36, 16.37 and 5.86, respectively ($O \approx 2 \times Ti + 3 \times W$). The results further confirm that the material is

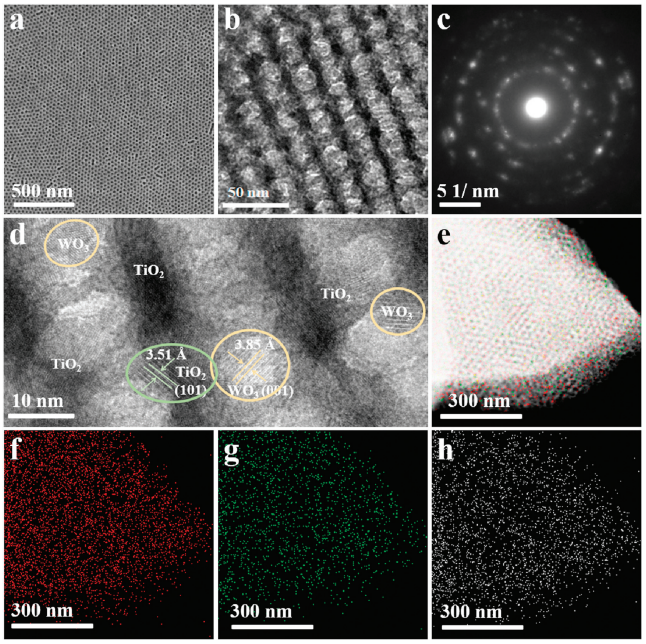

Fig. 2. (a) FESEM image, (b) TEM image, (c) SAED pattern, (d) HRTEM image, (e) STEM image and (f–h) the corresponding W, Ti, O elemental mapping images of the crystalline OM-TiO_2/WO_3 heterojunctions material obtained after heat treatment at 500 °C in air.

composed of TiO_2 and WO_3, indicating that the tungsten and titanium precursor can co-assemble in the EISA process. STEM image (Fig. 2e) and the elemental mapping images of Ti, W, and O elements (Figs. 2f-h) taken from the STEM area exhibit that these three elements are uniformly dispersed on the mesopore walls, thus further demonstrate that the uniform dispersion of TiO_2/WO_3 heterojunctions.

The nitrogen-sorption isotherms of the obtained OM-TiO_2/WO_3 heterojunctions (Fig. 1c) show a type IV curves of mesoporous materials. The sharp capillary condensation step appears at a large relative pressure (P/P_0) value of 0.85-0.90, demonstrating the large pore size of the obtained OM-TiO_2/WO_3 heterojunctions. Characteristic H1-type hysteresis loop is observed at the relative pressure (P/P_0) of ~0.70, indicating the large entrance size between conterminous spherical mesopores. The average pore size, BET surface area and corresponding pore volume of the OM-TiO_2/WO_3 heterojunctions are calculated to be 21.1 nm, 98 m^2/g and 0.28 cm^3/g, respectively (Fig. 1d).

The XPS survey spectra (Fig. 3) of the OM-TiO_2/WO_3 heterojunctions displays the existence of only W, Ti, O and C elements, in accordance with the EDX results. Figs. 3b-d show the high-resolution XPS spectra of Ti 2p, O 1s, and W 4d of the synthesized mesoporous TiO_2 and OM-TiO_2/WO_3 heterojunctions, respectively. The Ti 2p spectrum of OM-TiO_2/WO_3 heterojunctions show two peaks at 459.2 and 465.0 eV, respectively, corresponding to the $2p_{3/2}$ and $2p_{1/2}$ of Ti^{4+} ions (Fig. 3b) [43,44]. The peaks intensity and position of the OM-TiO_2/WO_3 heterojunctions show slight weakening and shift (0.4 eV) than the pure mesoporous TiO_2, attributing to the existence of TiO_2/WO_3 heterojunctions. In addition, the O 1s spectrum of OM-TiO_2/WO_3 heterojunctions also show broader peak than pure mesoporous TiO_2, further demonstrating the recombination between TiO_2 and WO_3 nanocrystals (Fig. 3c). Finally, the binding energy of W 4d peaks at 248.0 and 260.5 eV are also characteristic for W^{6+} oxidation state (Fig. 3d), suggesting the incorporated tungsten species in the OM-TiO_2/WO_3 and the oxidation state is +6.

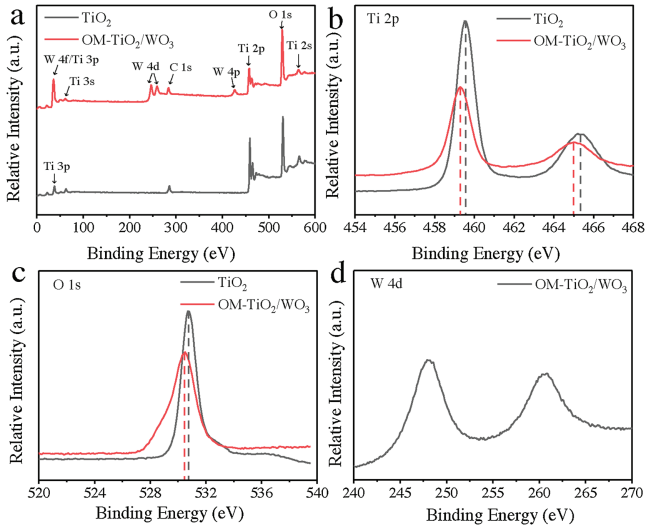

Fig. 3. (a) XPS spectra of the crystalline OM-TiO_2/WO_3 heterojunctions material and mesoporous TiO_2. High-resolution spectra of (b) Ti 2p, (c) O 1s, (d) W4d of OM-TiO_2/WO_3 and mesoporous TiO_2, respectively.

The synthesis condition of the mesoporous TiO_2/WO_3 was studied. First, the molar ratio of TIPO to WCl_6 (TIPO/WCl_6 = 1:3, 1:2, 1:1, 2:1, 3:1 and 4:1) was varied to investigate its effect on the resulting structure. The SAXS patterns (Fig. S5 in Supporting information) and the SEM images (Fig. S6 in Supporting informtion) of the TiO_2/WO_3 materials show that the ordered mesoporous structure can be formed at suitable ratios (TIPO/WCl_6 = 2:1-3:1). Excessive and insufficient addition of TIPO all lead to the disordered mesostructures. Second, Adjusting the amount of ethanol (10–60 wt% relative to THF), several samples can be obtained. With the increasement of additional ethanol from 10 wt% to 60 wt%, the number of the SAXS peaks increase firstly (Fig. S7 in Supporting information). Four scattering peaks can be observed when the dosage of ethanol is 40 wt%, demonstrating the highly ordered mesostructures. With the further increasement of additional ethanol, the number of the SAXS peaks decrease slightly, demonstrating the decreased periodicity of the mesostructures. The changing process of the periodicity can also be proved by the FESEM images (Fig. S8 in Supporting information).

Based on the above results, we speculate that the "acid-base pair" plays an importance role for the synthesis of final OM-TiO_2/WO_3 heterojunctions. In this system, WCl_6 was used as the "acid" and TIPO was used as the "base", respectively. WCl_6 dissolved in ethanol and was alcoholyzed to $WCl_{6-x}(OC_2H_5)_x$ (the "acid") which can react with the titanium precursor (Ti{$(OCH(CH_3)_2$}$_4$ (Ti(O-*i*-Pr)$_4$, the "base") and form the inorganic oligomers ([WCl_{6-x}/Ti(O-*i*-Pr)$_{4-y}$]$(OC_2H_5)_{x+y}$, the "acid-base pair"). The appropriate ratio of TIPO and WCl_6 is essential condition to provide a considerable amount of acid and alkali, which is conducive to form the stable "acid-base pair" completely. The formed "acid-base pair" can avoid the phase separation of single metal precursor from the homogeneous solution and can associate with the PEO segments of PEO-*b*-PS *via* hydrogen bonding, forming spherical composite micelles. As a consequence, an ordered mesostructures can be formed with the further evaporation of the co-solvent. In addition, the appropriate amount of ethanol is favorable to the formation and subsequent co-assembly process of the "acid-base pair". Less amount of additional ethanol cannot ensure the sufficient alcoholysis of WCl_6 which is unfavorable to the formation of "acid-base pair" completely. As a result, there is a part of the metal precursors will precipitate before assemble with the template, giving rise to only short-range ordered

mesostructures. In contrast, extra-amount of ethanol is unfavorable to the dissolution of PEO-*b*-PS and will lead to the precipitate of PEO-*b*-PS before assembly, giving rise to some defects and wormlike pores. Only when the dosage of ethanol is appropriate, the formed "acid-base pair" and PEO-*b*-PS can be co-assembly to ordered mesophase, forming large-domain ordered mesostructures. Consequently, by controlling the addition amount of TIPO and ethanol, OM-TiO_2/WO_3 heterojunctions can be obtained after subsequent processing.

The gas sensing performances of the OM-TiO_2/WO_3 heterojunctions have been investigated by using acetone as target analyte. The mesoporous TiO_2 and mesoporous TiO_2/WO_3 heterojunctions with different molar ratios of TiO_2 and WO_3 (TiO_2:WO_3 = 3:1, 14:1, denoted as OM-TiO_2/WO_3 and M-TiO_2/WO_3) are selected to investigate the effect of formed TiO_2/WO_3 heterojunctions on the sensing performance. The surface area of mesoporous TiO_2, M-TiO_2/WO_3 are 76 and 82 m^2/g, respectively. Meanwhile, the pore sizes of are 14.7 nm and 17.7 nm, respectively. The structure properties of three samples are listed in Fig. S9 and Table S2 (Supporting information). Firstly, the optimal working temperature of three sensors fabricated with TiO_2 and TiO_2/WO_3 heterojunctions is explored at 50 ppm acetone (Fig. S10 in Supporting information). The gas sensitivity of the OM-TiO_2/WO_3 with higher content of WO_3 and ordered mesostructures is much better than other materials. For all the materials, the optimum working temperature is 290 °C, so the temperature is selected as the operation temperature for next experiments. With the increase of temperature, much more thermal energy can be used to active the reaction between target gas molecules and the surface-chemisorbed oxygen species, thus is beneficial to the improvement of the sensor sensitivity. However, the surface-chemisorbed oxygen species will turn to desorption with the further increased temperature, thus leads to decreased sensing performance.

The gas-sensing properties of mesoporous TiO_2, OM-TiO_2/WO_3, and M-TiO_2/WO_3 heterojunctions sensors to different acetone concentrations at 290 °C were recorded (Fig. 4a). Three sensors all show good linear characteristic in a certain concentration range (Fig. 4b). The value of the gas response increased with the increasement of acetone concentration. Obviously, the OM-TiO_2/WO_3 heterojunctions exhibits much higher response to all acetone concentrations than pure mesoporous TiO_2 and the M-TiO_2/WO_3 heterojunctions with low content of WO_3. The response and recovery times of the obtained OM-TiO_2/WO_3 to 50 ppm acetone are about 3 s and 5 s, respectively (Fig. 4c). The response/recovery process was repeated four times and show excellent stability (Fig. 4d). Selectivity experiment demonstrate that the sensor based on TiO_2/WO_3 heterojunctions show excellent selectivity than other organic gases (H_2S, C_6H_6, CH_3OH, C_2H_5OH, HCHO, NH_3, H_2, CO, NO, CH_4) with the same concentration (50 ppm) and operating temperature of 290 °C (Fig. 4e). In addition, the evolution of the gas response toward 50 ppm acetone over 35 days is showed in Fig. 4f. During these days, the response value does not show any distinct difference, illustrating the excellent long-term stability. The superb selectivity and stability of the sensor give rise to promising practical applications in various fields. Up to now, there are rare reports about acetone sensors based on TiO_2/WO_3 heterojunctions. However, it will be interesting to compare the sensor performance based on OM-TiO_2/WO_3 heterojunctions with other sensor based on TiO_2 nanoparticle [45], TiO_2 nanorod [46], SnO_2-TiO_2 nanobelt heterostructure [47], NiO-decorated TiO_2 [48], TiO_2/WO_3 heterojunctions [49], *etc*. By comparison with above materials, the obtained OM-TiO_2/WO_3 exhibit much better performance than TiO_2 based gas sensor and other metal oxides composites (Table S3 in Supporting information).

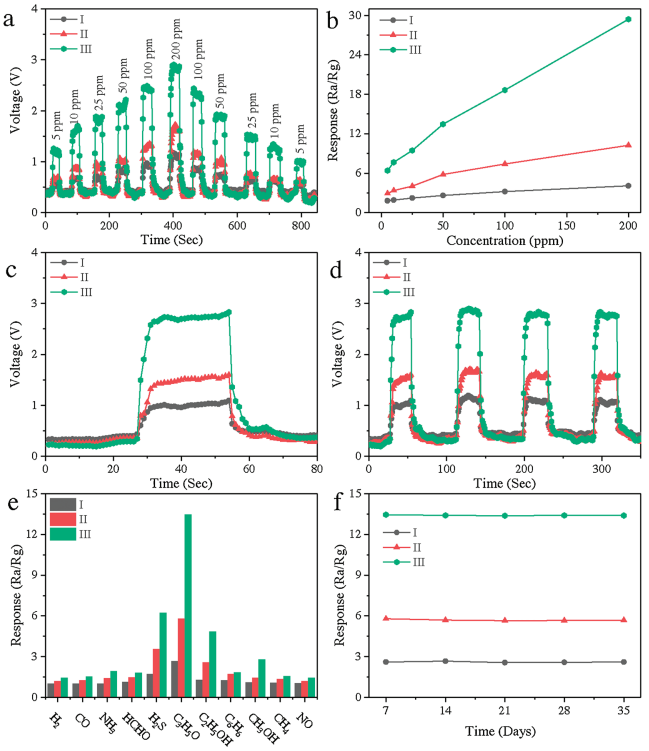

Fig. 4. The acetone sensing properties of sensors fabricated from the mesoporous TiO_2 (I), M-TiO_2/WO_3 (II), and OM-TiO_2/WO_3 (III) heterojunctions at an operating temperature of 290 °C. (a) dynamic response from 5 ppm to 200 ppm, (b) variation of gas response to different acetone concentrations from 5 ppm to 200 ppm, (c) the response/recovery time and (d) dynamic response-recovery cycles toward 50 ppm acetone gas, (e) response to different gases at 50 ppm, and (f) response of the sensor toward 50 ppm acetone, tested once a week.

According to the results of acetone-sensing tests, the OM-TiO_2/WO_3 heterojunctions exhibit superb gas sensing performance than others control samples, which are mainly attributed to the unique mesostructures and TiO_2/WO_3 heterojunctions. The high crystallinity nanocrystals and high surface area provide abundant bonding sites between target acetone and the surface-chemisorbed oxygen species on the sensing layer of mesoporous walls, improving the sensitivity of gas sensor. Large pore volume and interconnected mesopores are beneficial to the diffusion of acetone molecules in the mesostructures, improving the sensitivity and detection limit. In addition, the construction of TiO_2/WO_3 heterojunctions can induce the electrons transition from TiO_2 to WO_3 due to the better electrical conductivity of WO_3 [50]. When the OM-TiO_2/WO_3 heterojunctions sensor contacts with air atmosphere, more O_2 can be absorded on the surface of mesoporous walls and form abundant oxygen ions (O^{2-}, O^- and O_2^-) through the capture of e^- from TiO_2/WO_3 heterojunctions. Meanwhile, the increased resistance value can be detected of the sensor, attributing to the formed broadened electron depletion layer on the mesoporous walls. When the sensor is exposed to acetone at moderate temperature, chemical reaction happens between target gas and oxygen ions, forming CO_2 and H_2O. In this reaction, the formed oxygen ions get e^- from acetone and the e^- return to the conduction band of the sensor material, leading to a decreased resistance. The additional electrons generated by these enhanced surface reactions contributed to more sensitive signal response of the TiO_2/WO_3 heterojunctions-based sensors (Fig. S11 in Supporting information). Hence, TiO_2/WO_3 heterojunctions-based sensors can possess enhanced sensing performance to acetone.

In summary, highly ordered mesoporous TiO_2/WO_3 heterojunctions material was prepared through a "acid-base pair" adjusted EISA synthesis process. The WCl_6 and TIPO precursors were used as the "acid-base pair" and PEO-*b*-PS was used as the soft template. The formation of "acid-base pair" was effective to adjust the hydrolysis and condensation process of used inorganic precursors, thus makes the co-assembly process more controllable. In addition, PEO-*b*-PS can be converted to rigid carbon which can protect the mesostructures from collapse during the crystallization process. The resultant OM-TiO_2/WO_3 heterojunctions exhibits highly crystalline TiO_2/WO_3 heterojunctions frameworks, large pore size (~21.1 nm), high surface areas (98 m^2/g), and high pore volume (0.28 cm^3/g). When being used as a sensor for acetone, the OM-TiO_2/WO_3 heterojunctions show excellent response/recovery performance (3 s/5 s), outstanding linear dependence, repeatability, selectivity, and long-term stability (35 days). The extraordinary performances are attributed to the synergistic coupling effect between high crystalline TiO_2/WO_3 heterojunctions, high surface areas, and accessible large pores. This work provided a new avenue to construct highly ordered mesoporous metal oxides heterojunctions for gas sensing applications.

Acknowledgments

This work was supported by the National Natural Science Foundation of China (Nos. 51822202 and 51772050), China Postdoctoral Science Foundation (No. 2019M651342), Shanghai Rising-Star Program (No. 18QA1400100), Youth Top-notch Talent Support Program of Shanghai, the Shanghai Committee of Science and Technology, China (No. 19520713200), DHU Distinguished Young Professor Program and Fundamental Research Funds for the Central Universities.

Appendix A. Supplementary data

Supplementary material related to this article can be found, in the online version, at doi:https://doi.org/10.1016/j.cclet.2019.08.042.

References

[1] Y. Li, W. Luo, N. Qin, et al., Angew. Chem. Int. Ed. 53 (2014) 9035–9040.
[2] J. Ma, Y. Ren, X. Zhou, et al., Adv. Funct. Mater. 28 (2018) 1705268.
[3] Y. Zhu, Y. Zhao, J. Ma, et al., J. Am. Chem. Soc. 139 (2017) 10365–10373.
[4] X. Zhou, Y. Zhu, W. Luo, et al., J. Mater. Chem. A: Mater. Energy Sustain. 4 (2016) 15064–15071.
[5] Y. Ren, X. Zhou, W. Luo, et al., Chem. Mater. 28 (2016) 7997–8005.
[6] Z. Wang, Y. Zhu, W. Luo, et al., Chem. Mater. 28 (2016) 7773–7780.
[7] M. Tiemann, Chem. Eur. J. 13 (2007) 8376–8388.
[8] T. Wagner, S. Haffer, C. Weinberger, D. Klaus, M. Tiemann, Chem. Soc. Rev. 42 (2013) 4036–4053.
[9] A. Gurlo, Nanoscale 3 (2011) 154–165.
[10] Z. Wang, Z. Tian, D. Han, F. Gu, ACS Appl. Mater. Interf. 8 (2016) 5466–5474.
[11] G. Sakai, N. Matsunaga, K. Shimanoe, N. Yamazoe, Sens. Actuat. B: Chem 80 (2001) 125–131.
[12] A. Cabot, J. Arbiol, J.R. Morante, et al., Sens. Actuat. B: Chem 70 (2000) 87–100.
[13] W. Li, J. Yang, Z. Wu, et al., J. Am. Chem. Soc. 134 (2012) 11864–11867.
[14] Y. Liu, K. Lan, S. Li, et al., J. Am. Chem. Soc. 139 (2017) 517–526.
[15] N. Pinna, G. Neri, M. Antonietti, M. Niederberger, Angew. Chem. Int. Ed. 43 (2004) 4345–4349.
[16] W. Wang, K. Zhang, Y. Yang, et al., Microporous Mesoporous Mater. 193 (2014) 47–53.
[17] R. Zhao, F. Guo, Y. Hu, H. Zhao, Microporous Mesoporous Mater. 93 (2006) 212–216.
[18] G. Korotcenkov, I. Blinov, M. Ivanov, J.R. Stetter, Sens. Actuat. B: Chem 120 (2007) 679–686.
[19] M. Pal, L. Wan, Y. Zhu, et al., J. Colloid Interface Sci. 479 (2016) 150–159.
[20] Y. Zhang, Y. Shi, Y.H. Liou, et al., J. Mater. Chem. 20 (2010) 4162–4167.
[21] H. Yoshitake, T. Sugihara, T. Tatsumi, Chem. Mater. 14 (2002) 1023–1029.
[22] Y. Liu, E. Koep, M. Liu, Chem. Mater. 17 (2005) 3997–4000.
[23] Y. Zou, X. Zhou, Y. Zhu, et al., Acc. Chem. Res. 52 (2019) 714–725.
[24] C. Wang, Y. Zhao, L. Zhou, et al., J. Mater. Chem. A: Mater. Energy Sustain. 6 (2018) 21550–21557.
[25] J. Wei, Y. Ren, W. Luo, et al., Chem. Mater. 29 (2017) 2211–2217.
[26] Y. Li, X. Zhou, W. Luo, et al., Adv. Mater. Interfaces 6 (2019) 1801269.
[27] J. Zhang, Y. Deng, D. Gu, et al., Adv. Energy Mater. 1 (2011) 241–248.
[28] D. Gu, F. Schuth, Chem. Soc. Rev. 43 (2014) 313–344.
[29] X. Sun, Y. Shi, P. Zhang, et al., J. Am. Chem. Soc. 133 (2011) 14542–14545.
[30] W. Li, J. Liu, D. Zhao, Nat. Rev. Mater. 1 (2016) 16023.
[31] F. Jiao, A.H. Hill, A. Harrison, et al., J. Am. Chem. Soc. 130 (2008) 5262–5266.
[32] H. Liu, G.X. Wang, J. Liu, S.Z. Qiao, H.J. Ahn, J. Mater. Chem. 21 (2011) 3046–3052.
[33] Y. Shi, B. Guo, S.A. Corr, et al., Nano Lett. 9 (2009) 4215–4220.
[34] J. Roggenbuck, M. Tiemann, J. Am. Chem. Soc. 127 (2005) 1096–1097.
[35] D. Zhao, J. Feng, Q. Huo, et al., Science 279 (1998) 548–552.
[36] Y. Meng, D. Gu, F. Zhang, et al., Angew. Chem. Int. Ed. 44 (2005) 7053–7059.
[37] Y. Liu, Z. Wang, W. Teng, et al., J. Mater. Chem. A: Mater. Energy Sustain. 6 (2018) 3162–3170.
[38] P. Yang, D. Zhao, D.I. Margolese, B.F. Chmelka, G.D. Stucky, Nature 396 (1998) 152–155.
[39] H.S. Yun, K. Miyazawa, H.S. Zhou, I. Honma, M. Kuwabara, Adv. Mater. 13 (2001) 1377–1380.
[40] F. Schüth, Chem. Mater. 13 (2001) 3184–3195.
[41] W.T. Koo, S.J. Choi, S.J. Kim, et al., J. Am. Chem. Soc. 138 (2016) 13431–13437.
[42] B. Tian, X. Liu, B. Tu, et al., Nat. Mater. 2 (2003) 159–163.
[43] Z. Chen, L. Xu, Q. Chen, et al., J. Mater. Chem. A: Mater. Energy Sustain. 7 (2019) 6740–6746.
[44] D. Guan, Q. Yu, C. Xu, et al., Nano Res. 10 (2017) 4351–4359.
[45] R. Rella, J. Spadavecchia, M.G. Manera, et al., Sens. Actuat. B: Chem 127 (2007) 426–431.
[46] H. Bian, S. Ma, A. Sun, et al., Superlattices Microstruct. 81 (2015) 107–113.
[47] X. Wang, Y. Sang, D. Wang, S. Ji, H. Liu, J. Alloys. Compd. 639 (2015) 571–576.
[48] G.J. Sun, H. Kheel, S. Park, et al., Ceram. Int. 42 (2016) 1063–1069.
[49] M. Epifani, E. Comini, R. Díaz, et al., J. Alloys. Compd. 665 (2016) 345–351.
[50] X. Liu, K. Pan, L. Wang, et al., RSC Adv. 5 (2015) 96539–96546.